Journal of Catalysis 262 (2009) 294–303

Contents lists available at ScienceDirect

Journal of Catalysis

www.elsevier.com/locate/jcat

Water–gas-shift reaction on a $Ni_2P(001)$ catalyst: Formation of oxy-phosphides and highly active reaction sites

Ping Liu [a,*], José A. Rodriguez [b], Yoshiro Takahashi [c], Kenichi Nakamura [c]

[a] Center for Functional Nanomaterials, Brookhaven National Laboratory, Upton, NY 11973, USA
[b] Department of Chemistry, Brookhaven National Laborator, Upton, NY 11973, USA
[c] Materials and Structures Laboratory, Tokyo Institute of Technology, Yokohama 226-8503, Japan

ARTICLE INFO

Article history:
Received 5 November 2008
Revised 7 January 2009
Accepted 9 January 2009
Available online 29 January 2009

Keywords:
Water–gas-shift
Nickel phosphide
Hydrogen production
Reaction mechanism

ABSTRACT

The water–gas-shift (WGS, $CO + H_2O \rightarrow H_2 + CO_2$) reaction was studied on the $Ni_2P(001)$ surface using a combination of experimental and theoretical methods. Our experimental measurements show that $Ni_2P(001)$ displays an activity larger than that of Ni(100) or even Cu(100), which is the best metal catalyst for the WGS process. The good behavior of Ni_2P is associated with the Ni oxy-phosphides formed as a result of strong O ↔ P interactions. Under reaction conditions, most of the P sites of $Ni_2P(001)$ are covered with oxygen. The addition of Cs to the nickel phosphide surface increases the saturation coverage of oxygen and enhances catalytic activity. As in the case of a [NiFe] hydrogenase enzyme, the active sites of $O/Ni_2P(001)$ involve the combination of a metal and a light atom. This configuration of the active sites leads to significant changes in the reaction mechanism with respect to that on Ni(100) or Cu(100). The O atoms on the $Ni_2P(001)$ surface facilitate the WGS reaction in both direct and indirect ways. On one hand, O helps to lower the barrier for water dissociation; on the other hand, it also deactivates the Ni sites in the surface to provide moderate bonding to the adsorbates, and the barriers for each elementary step in the WGS process become lower than 1.2 eV. Our results imply that the high performances of catalysts in the WGS rely heavily on the cooperation between oxygen and metal centers with moderate activity.

Published by Elsevier Inc.

1. Introduction

With fossil fuels in limited supply, hydrogen has been recognized as an environmentally acceptable, alternative energy carrier. Furthermore, the reaction of hydrogen with CO or CO_2 can lead to the generation of liquid fuels which contain heavy alcohols or alkanes (Fischer–Tropsch process). Thus, there is a broad interest in optimizing different routes used for the production of hydrogen. The water–gas-shift (WGS) reaction is an important step in several industrial processes [1,2]. The overall reaction corresponds to the conversion of carbon monoxide and water into carbon dioxide and hydrogen ($CO + H_2O \rightarrow CO_2 + H_2$). It is primarily used to increase the H_2 content as well as reducing the CO concentration in synthesis gas and is an essential part of a hydrogen plant [2]. In recent years, the WGS reaction at low temperature has redrawn attention due to its application in fuel cell technology [3]. The typical industrial catalyst for the low-temperature WGS reaction is Cu [4–9] with ZnO and Al_2O_3 as support materials [10,11]. However, there are problems in using these systems for automotive applications since they are pyrophoric [11] and can be deactivated by the condensation of water [12].

Extensive studies, involving theory and/or experiment, have been carried out to search for new WGS catalysts to replace the commercial Cu-based catalyst. The disadvantages of the industrial catalysts can be overcome by the use of precious metal based systems: pure metals (Pd, Au, Pt) [13–16], and alloys [17,18]. However, besides the factor of cost, the deactivation of the catalysts was also found under the working conditions of the WGS reaction [19–21]. Recently, it has been reported that the WGS activities of metal (Au, Cu, Pt, Pd) catalysts are promoted significantly by forming composite materials with oxides (CeO_2, TiO_2, MoO_2): metal nanoparticles supported on oxides and oxide nanoparticles supported on metals [22–25]. These systems operate as bifunctional catalysts, taking advantage of the properties of the metal and oxide, and the WGS reaction runs fast at the interface [25].

It is worthwhile to study the WGS reaction on compounds which involve non-expensive metals and light elements (C, N, P, S). In principle, the formation of these compounds can lead to special catalytic properties due to ensemble (i.e. reduction in the number of exposed metal centers) or ligand effects (i.e. metal → light ele-

* Corresponding author.
E-mail address: pingliu3@bnl.gov (P. Liu).

0021-9517/$ – see front matter Published by Elsevier Inc.
doi:10.1016/j.jcat.2009.01.006

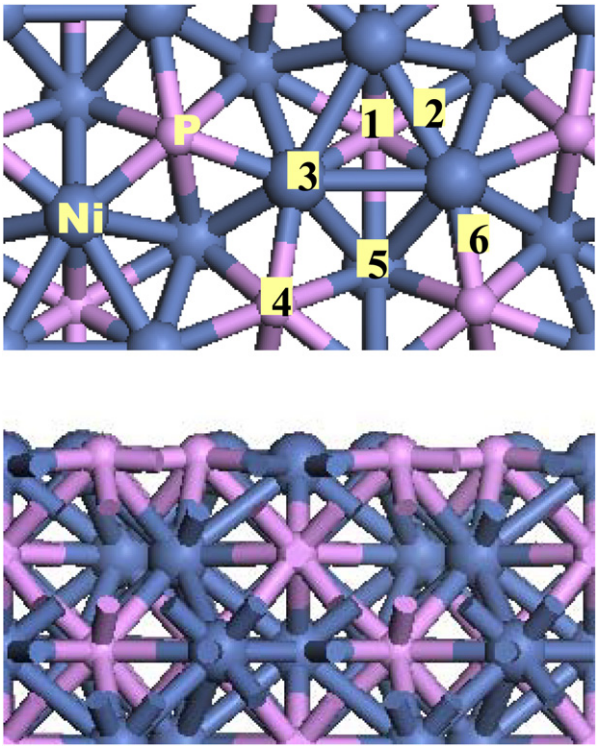

Fig. 1. (Color) Optimized geometries of the $Ni_2P(001)$ surface. (Upper panel) Top view; (lower panel) side view. Different adsorption sites on each surface are labeled by Nos. 1–6. 1: metal hollow; 2: metal bridge; 3: metal atop; 4: phosphorus atop; 5: hydrid metal–phosphorus hollow; 6: hydrid metal–phosphorus bridge.

ment charge transfer) [26–33]. Interestingly, Mo_2C has been found to display a higher WGS activity than the industrial Cu-based catalyst [26,29], but this carbide has problems of long-term stability. A recent theoretical study has investigated the hydrogen evolution reaction (HER, $2H^+ + 2e^- \rightarrow H_2$) on a [NiFe] hydrogenase enzyme, $[Ni(PS3^*)(CO)]^{-1}$ and $[Ni(PNP)_2]^{2+}$ complexes, and surfaces such as Ni(111), Pt(111) or $Ni_2P(001)$ [30]. The calculations suggest that among all the systems investigated, Ni_2P should be the best practical catalyst for the HER, combining the high thermostability of the surfaces and the high catalytic activity of the [NiFe] hydrogenase [30]. Furthermore, Ni_2P exhibits an extremely high activity for catalyzing hydrodesulfurization processes [28,34–37]. In the present paper, we report, for the first time, experiments and density functional theory (DFT) calculations for the WGS reaction on a $Ni_2P(001)$ surface (Fig. 1). The (001) plane is of great relevance because it is the predominant orientation observed in real catalysts containing Ni_2P crystallites on a silica support [34,37]. Our experiments show that, under similar experimental conditions, Ni_2P displays a WGS activity larger than that of Ni or the best metal catalysts for the reaction, Cu. The catalytic activity of $Ni_2P(001)$ can be substantially enhanced by adding a small amount of cesium to the phosphide surface. According to our DFT calculations, the active phase of Ni_2P towards the WGS reaction is a Ni oxy-phosphide, where both O and P are not spectators and participate in the reaction directly. Although Ni_2P has metallic character [28], the mechanism seen for the WGS reaction on $Ni_2P(001)$ shows important differences with respect to that found on Cu(100) or Cu(111) [8,9], as the active sites of the metal phosphide resemble those of a [NiFe] hydrogenase enzyme.

2. Experimental and theoretical methods

2.1. Experimental studies

The experimental data presented in Section 3 were collected in a conventional ultrahigh-vacuum (UHV) chamber (base pressure $\sim 1 \times 10^{-10}$ Torr) equipped with instrumentation for X-ray photoelectron spectroscopy (XPS. Mg or Al$K\alpha$ X-ray source), low-energy electron diffraction (LEED), ion scattering spectroscopy (ISS), Auger electron spectroscopy (AES), and temperature programmed desorption (TPD) [28]. The UHV chamber had attached a high-pressure cell or batch reactor [5,6,24,25]. In our studies, the sample was transferred between the reactor and vacuum chamber without exposure to air.

The $Ni_2P(001)$ crystal, 9 mm in diameter and 1 mm in thickness, was prepared at the Tokyo Institute of Technology. The $Ni_2P(001)$ crystal was mounted in a manipulator that allowed cooling to 100 K, resistive heating to 1400 K, and e-beam heating to 2500 K. Clean $Ni_2P(001)$ surfaces were prepared following a procedure similar to that reported in Ref. [28]. Ion bombardment and annealing in UHV at 750 K produced ordered (1×1) hexagonal surfaces that have a composition close to that expected for bulk Ni_2P [28]. Ion bombardment with Ar^+ at 300 K removed surface impurities like C and O plus P atoms, producing Ni-rich surfaces. Surfaces with the correct stoichiometry were produced by annealing in UHV at temperatures above 700 K (diffusion of P from the bulk to the surface) [28] or by reaction with small amounts of PH_3 gas at 500–600 K. Along the (001) direction of bulk Ni_2P, there is an alternation of planes that have Ni_3P and Ni_3P_2 compositions [28,30]. A two-plane repeat unit along the (001) direction gives the bulk Ni_2P stoichiometry. LEED, ISS and scanning tunneling microscopy (STM) showed that the $Ni_2P(001)$ surfaces used in this study exposed mainly Ni_3P_2 planes (see Fig. 1) [31–33]. In these surfaces, the area exposing Ni_3P planes was in the range of 10–20% of the total surface area. This is consistent with the results of DFT calculations which indicate that a Ni_3P_2 termination has a lower surface-free energy than a Ni_3P termination [27,28].

In a set of experiments, the catalytic activity of $Ni_2P(001)$ was enhanced by depositing on the surface small amounts of cesium. Cesium was vapor deposited on the Ni_2P substrate by heating a SAES getter chromate source. For small doses, the relative coverage of Cs (Θ_{Cs}) was determined by comparing the area under the Cs 3d XPS peaks to the corresponding area for a saturated monolayer of Cs on $Ni_2P(001)$ at 300 K.

In the kinetic measurements the sample was transferred to the batch reactor at ~300 K, then the reactant gases were introduced (20 Torr of CO and 10 Torr of H_2O) and the sample was rapidly heated to the reaction temperature (575, 600, 625 or 650 K). The reaction conditions used to test the catalytic activity of the nickel phosphide samples were similar to those used in previous studies examining the WGS reaction on well-defined surfaces [5,6,15,24,25]. The CO gas was cleaned of any metal carbonyl impurity by passing it through purification traps. Product yields were analyzed by a gas chromatograph [24,25]. The amount of molecules produced was normalized by the area of the sample which was exposed to the reactants inside the batch reactor. The sample holder was passivated by extensive sulfur poisoning (exposure to H_2S) and have no catalytic activity. In our reactor a steady-state regime for the production of H_2 and CO_2 was reached before 3 min of reaction time, and then a constant reaction rate was seen for periods as long as 70 min. The kinetic experiments were done in the limit of low conversion (<10%). After the tests of catalytic activity the surfaces of the catalysts were characterized using XPS and/or ISS. The gases were pumped out from the reactor, and the sample was transferred back to the UHV chamber while it was cooling to room temperature.

2.2. Theoretical studies

The DFT calculations were performed using the CASTEP (Cambridge Serial Total Energy Package) suite of programs [38], which have proved to be very useful in theoretical studies dealing with metal and metal phosphide surfaces [28,39,40]. Similar calculations have successfully described the WGS reaction on metal surfaces, metal nanoparticles and metal carbides [8,24,25,29]. The Kohn–Sham one-electron equations were solved on a basis set of plane waves with kinetic energy below 25Ry and ultra-soft pseudopotentials were used to describe the ionic cores [41]. Brillouin zone integration was approximated by a sum over special k-points selected using the Monkhorst–Pack scheme [42]. Enough k-points ($5 \times 5 \times 1$) were chosen to make sure that there was no significant change in the calculated energies when a larger number of K points was used. The exchange-correlation energy and the potential were described by the revised version of the Perdew–Burke–Ernzerhof (RPBE) functional [43]. Previous DFT calculations using the RPBE functional predicted adsorption energies for CO, S, SO_2 and thiophene on metal and metal phosphide surfaces were very close to those measured experimentally ($|\Delta E| < 0.25$ eV) [28,39,40]. Using this setup, our calculated lattice parameters for Ni_2P (hexagonal, $a = b = 5.93$ Å, $c = 3.37$ Å) agrees well with the experiments ($|\Delta d| < 0.06$ Å) [44,45].

The $Ni_2P(001)$ crystal used in the experimental studies exposed mainly Ni_3P_2 planes (see above). To model a $Ni_2P(001)$ surface in a Ni_3P_2-termination, Fig. 1, we used four-layer slabs [28,39,40], repeated in a supercell geometry with a 11 Å vacuum between the slabs. The $Ni_2P(001)$ substrate was represented by a $\sqrt{3} \times \sqrt{3}$ unit cell, corresponding to a surface coverage of 1/3 of a monolayer (ML). In the calculations, the top three layers were allowed to relax in all dimensions together with the adsorbates, while the bottom layer was kept fixed at the calculated bulk positions. We checked the effect of slab thickness and number of relaxed layers on the energetics for the strong O adsorption. The results showed that the adsorption energy using four layer and six layer slabs were consistent. Due to the strong O–Ni_2P interaction as shown below, the energy levels off only when the top three layers are allowed to relax, where the adsorption energy increases by 0.16 eV from top 1 layer relaxed to top 2 layer relaxed and 0.03 eV from top 2 layers relaxed to top 3 layers relaxed. The methodology used in this article is similar to that used by our group in previous studies of $Ni_2P(001)$ [28,30].

3. Results and discussion

3.1. Activity of $Ni_2P(001)$ and $Cs/Ni_2P(001)$ for the water–gas shift: Experimental studies

As discussed above, the (001) surface of nickel phosphide contains both Ni and P centers (Fig. 1). After exposing this substrate to a mixture of H_2O (10 Torr) and CO (20 Torr) in the high-pressure reactor, O 1s XPS spectra showed the presence of adsorbed oxygen. Fig. 2 displays the variation of the O 1s signal as a function of reaction time for two different temperatures (575 and 650 K). In these experiments the $Ni_2P(001)$ surface was expose to the mixture of H_2O/CO during the indicated period of time, then the gases were pumped out, and the corresponding O 1s spectrum was collected while the sample was cooling to room temperature. The amount of adsorbed oxygen increased up to a reaction time of ~3 min when it reached saturation. The P 2p XPS spectrum of clean $Ni_2P(001)$ exhibited the main peak at ~129.9 eV. Upon the adsorption of a saturation coverage of O, the total intensity of the P 2p features decreased, with a broadening towards the high binding energy side. After curve-fitting [23], the P 2p spectra, a small peak appeared at ~131.6 eV (ΔBE ~ 1.7 eV) consistent with the formation of P–O

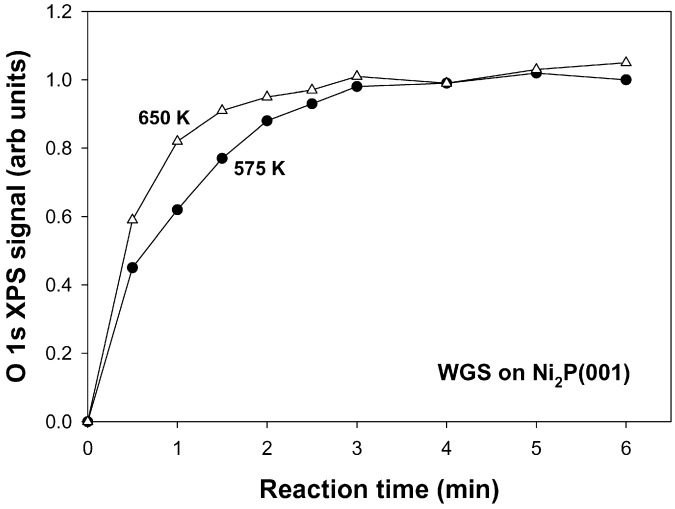

Fig. 2. Variation of the oxygen coverage (O 1s signal in XPS) with reaction time after exposing a $Ni_2P(001)$ surface to a mixture of H_2O (10 Torr) and CO (20 Torr) at 575 and 650 K.

bonds on the surface [46]. The adsorption of oxygen had a relatively minor effect on the position (ΔBE ~ 0.4 eV) of the Ni 2p signal in XPS. In ISS, a saturation coverage of O induced a decrease of ~89% in the P signal and a decrease of only 38% in the Ni signal. Thus, it appears that the O deposited on $Ni_2P(001)$ by the full dissociation of water interacted mainly with the P atoms to generate an oxy-phosphide. In principle, the uncovered Ni sites detected by ISS, ~62% of those exposed by a clean $Ni_2P(001)$ surface, were available for participating in the WGS process. However, after exposing $Ni_2P(001)$ and the $O/Ni_2P(001)$ surfaces to carbon monoxide at 140 K, the amount of CO adsorbed on the O covered systems was ~40% of that seen on a clean $Ni_2P(001)$ substrate.

The presence of O on the Ni_2P surface does not imply that this system will not be catalytically active. For example, it has been reported that Ni_2P substrates partially covered with S are excellent catalysts for hydrodesulfuration [28,34,36]. We found that the $O/Ni_2P(001)$ surfaces generated in the experiments of Fig. 2 did catalyze the WGS. Steady-state was easily achieved and we did not observe deactivation of the catalysts after 70 min of operation. Under reaction conditions no additional O was deposited on the phosphide surface. Thus, the exposed Ni sites were not oxidized. There was a very small amount of C at a binding energy of ~289.7 eV which could be attributed to HCOO or CO_x species on the catalyst surface [47]. Similar C 1s features were observed after carrying out the WGS on metal/oxide catalysts [15,24,48], but their concentration on the oxy-phosphide was 3–4 times smaller. The XPS data did not provide a clear evidence for the participation of HCOO or CO_x in the main reaction path for the WGS on $Ni_2P(001)$. Using the ln of the measured reaction rates for the WGS on $Ni_2P(001)$ at 575, 600, 625 and 650 K, we constructed the Arrhenius plot shown in the bottom panel of Fig. 3. This plot yields an apparent activation energy of 12.7 kcal/mol for the WGS on $Ni_2P(001)$.

Fig. 4 compares the WGS activity found for $Ni_2P(001)$ with that detected for Ni(100) and Cu(100) [24]. Copper is the best known metal catalyst for the WGS [4–9,14]. Nickel has a lower activity than copper because it binds the intermediates of the WGS too strongly [14]. The Ni(100) surface is deactivated by a layer of carbon (in a "carbidic" state) formed by the Boudouard reaction, $2CO(gas) \rightarrow C(ads) + CO_2(gas)$ [7]. The water in the reaction mixture for the WGS did not oxidize the Ni atoms present in $Ni_2P(001)$ or Ni(100). Post-reaction surface characterization with XPS showed quite small amounts of O or C on Cu(001) [24]. The metal surfaces did not exhibit the photoemission peaks characteristic of HCOO or

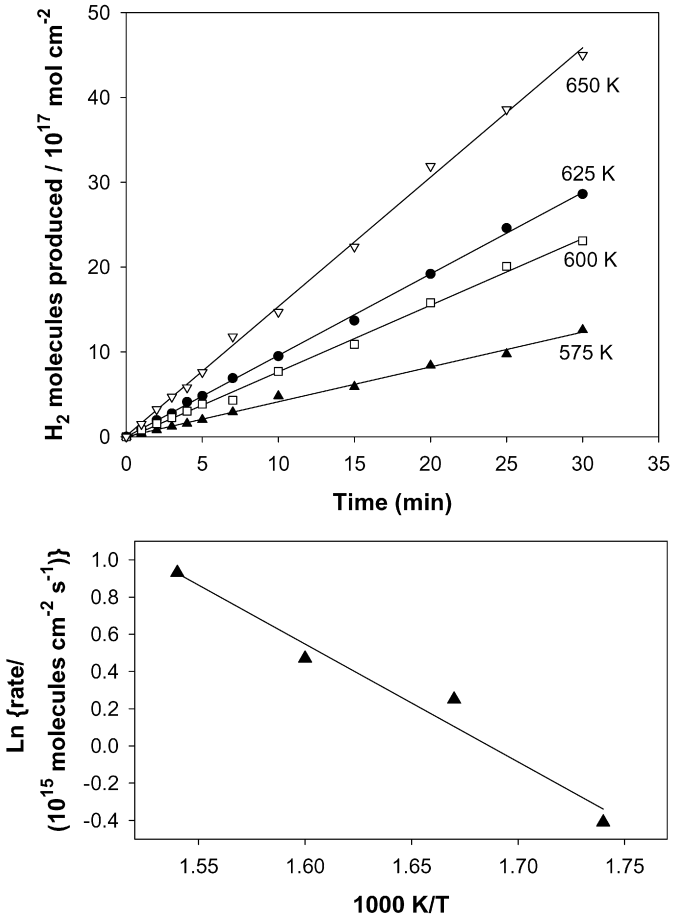

Fig. 3. (Top panel) Amount of H_2 produced through the WGS on $Ni_2P(001)$ at 575, 600, 625 and 650 K. Before $t = 0$ min, the $Ni_2P(001)$ surface was exposed to a reaction mixture of H_2O (10 Torr) and CO (20 Torr) for 5 min. (Bottom panel) Arrhenius plot for the rate of the WGS on Ni2P(001). The plot was constructed using steady-state rates obtained from the data displayed in the top panel.

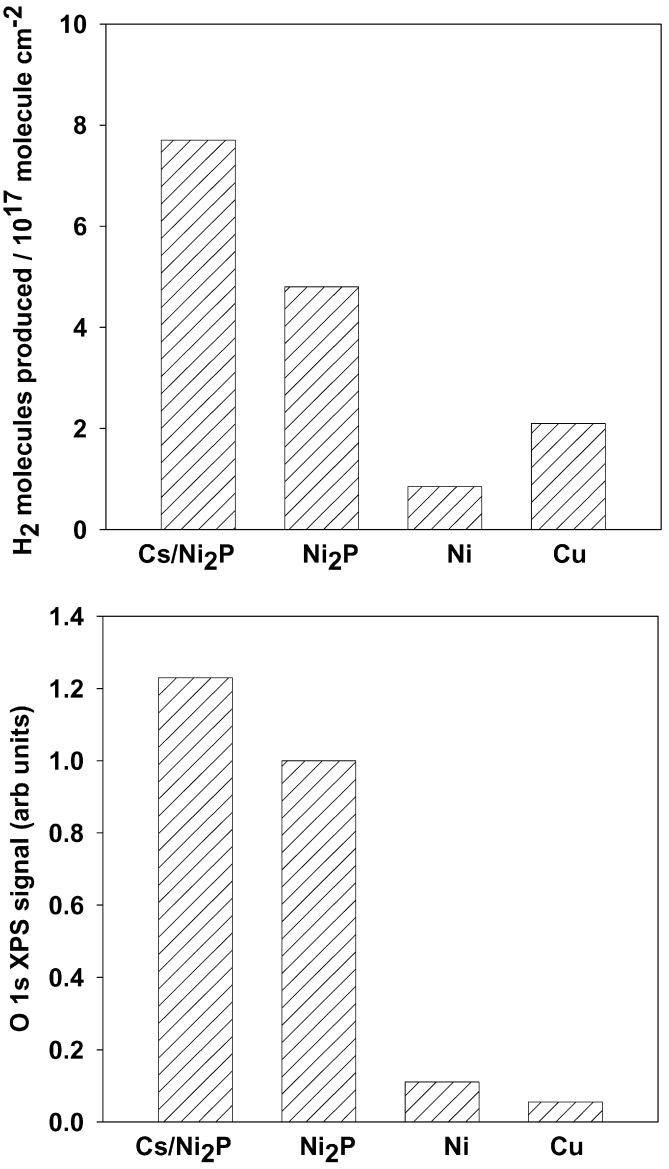

Fig. 4. (Top panel) Amount of H_2 produced on $Cs/Ni_2P(001)$, $Ni_2P(001)$, Ni(100) and Cu(100) after 5 min under a steady-state rate at 625 K, 20 Torr of CO and 10 Torr of H_2O. (Bottom panel) O 1s XPS signal measured after performing the WGS on the indicated surfaces.

CO_x species [5,6,24]. As we will see in the next section, the formation of Ni–P bonds and the subsequent adsorption of oxygen moderates the chemical reactivity of $Ni_2P(001)$ making it more catalytically active than Ni(100) and Cu(100). $O/Ni_2P(001)$ is a good WGS catalyst because it obeys Sabatier principle: It interacts well with the reactants without binding the intermediates or products too strongly. It is difficult to define the exact number of active sites present on the $O/Ni_2P(001)$ catalyst. In experiments of CO chemisorption at 140 K, we found that the amount of CO adsorbed on $O/Ni_2P(001)$ was 0.2–0.3 times the amount seen on Cu(100). If the rates in the top panel of Fig. 4 are normalized by the number of metal sites titrated by CO chemisorption, it will appear that $O/Ni_2P(001)$ is 7–9 times more active than Cu(100). However, in this comparison one must be careful because the active sites in $O/Ni_2P(001)$ do involve a particular combination of metal and O centers, see Section 3.2.3, and CO chemisorption may be overestimating their concentration because the molecule will bind to all free metal sites. The modification of Ni_2P by the adsorption of O produces catalysts that are very active for the WGS, while a modification by the adsorption of S leads to excellent catalysts for hydrodesulfurization [28,34,36].

Cesium is a well-known promoter of Cu-based WGS catalysts [1,5,6]. After depositing 0.15 monolayers of Cs on $Ni_2P(001)$, we found a substantial enhancement in the catalytic activity (top panel in Fig. 4). Cs 3d XPS spectra indicated that during reaction the Cs was probably transformed into a CsO_x or $Cs(OH)_x$ species [5]. Overall, there was an increase in the saturation coverage of O on the nickel phosphide surface. For the systems in Fig. 4 high catalytic activity correlates with a large coverage of oxygen. The DFT calculations discussed below show that oxygen helps the energetics for the WGS by reducing the barrier for the dissociation of water.

In Fig. 5 we can see that $Ni_2P(001)$ and $Cs/Ni_2P(001)$ have an activity comparable or better than that of Cu nanoparticles supported on ZnO(000$\bar{1}$) [24]. This is quite remarkable, since we are dealing with extended surfaces of nickel phosphide and Cu/ZnO is a system used for catalyzing the WGS in industrial applications [1]. In Fig. 5, the systems containing Cu nanoparticles {$Cu/CeO_2(111)$, Cu/ZnO(000$\bar{1}$), Cu/MgO(100)} [15,24] expose more free metal centers than the $Ni_2P(001)$ and $Cs/Ni_2P(001)$ catalysts which are partially covered with oxygen. In experiments of CO chemisorption, the amount of CO adsorbed on the Cu/ZnO(000$\bar{1}$) and $Cu/CeO_2(111)$ catalysts at 140 K was 1.1–1.4 times larger than the amount adsorbed on the $Ni_2P(001)$ and $Cs/Ni_2P(001)$ catalysts. The apparent activation energy for the WGS on each catalyst may be a good parameter to quantify relative catalytic activity [4–7,15,24].

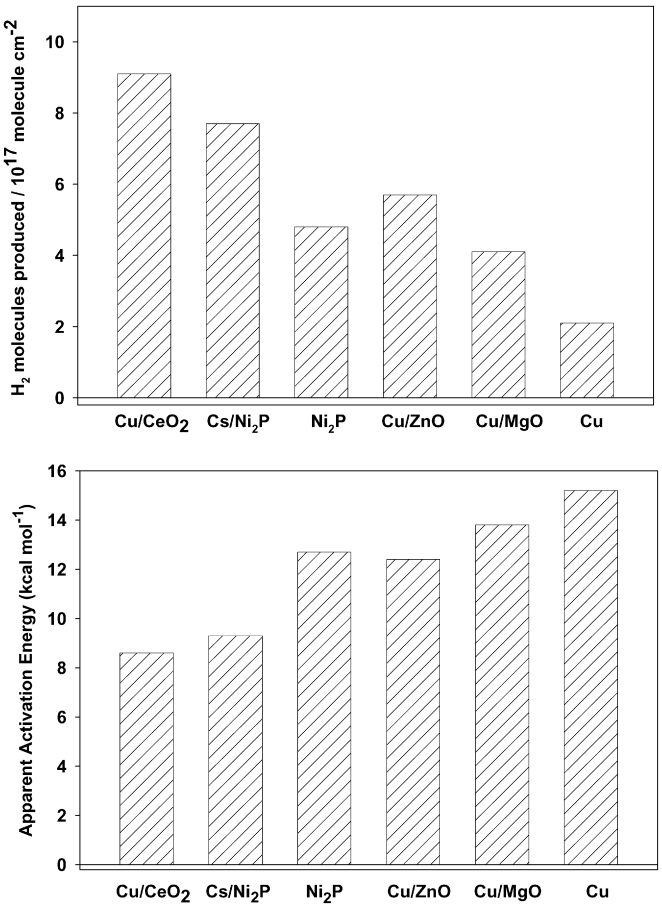

Fig. 5. (Top) H_2 produced under a steady-state rate for the WGS (20 Torr of CO, 10 Torr of H_2O, 625 K, 5 min) on $Cu/CeO_2(111)$ [20], $Cs/Ni_2P(001)$, $Ni_2P(001)$, Cu/ZnO(000i), Cu/MgO(001), and Cu(100). (Bottom) Corresponding apparent activation energies for the WGS on the indicated surfaces.

$Cs/Ni_2P(001)$ and $Cu/CeO_2(111)$ exhibit the lowest apparent activation energies and the highest production of H_2 per surface area.

3.2. Mechanism of the WGS on $Ni_2P(001)$: Theoretical studies

Previous theoretical works have studied the mechanism of the WGS on metals [8,9,13] or metal/oxide surfaces [25]. The Ni–P bonds in nickel phosphide have a low degree of ionicity and the compound has metallic character [28]. The presence of metal and phosphorous sites in the $Ni_2P(001)$ surface makes this system different from Cu(100) or Cu(111). The nickel phosphide substrate has binding sites that in many aspects are similar to those of a [NiFe] hydrogenase enzyme [30]. However, it is frequently assumed that the P sites in metal phosphide catalysts are simple spectators [34,37,45]. We will begin this section by examining the adsorption energies of the reactants and products of the WGS on different sites of $Ni_2P(001)$ and comparing these adsorption energies to those on Ni(111) and Cu(111).

3.2.1. Calculated adsorption energies

Table 1 includes the calculated adsorption energies for H_2, CO, H_2O, OH, O_2 and CO_2 on the Ni(111) surface. The corresponding adsorption energies for the case of Cu(111) have been calculated in our previous study using the same method [8,29]. One can see that the energies from the present calculations are in good agreement with the experiments and other theoretical studies [9,13,43,49–52]. As observed previously [9,13,49,53], the present calculations show that H_2, O_2, OH and CO are always found to be the most stable at

Table 1
Calculated energies (eV) for the preferential adsorptions at low coverage on the surfaces of Cu(111), Ni(111), $Ni_2P(001)$ and O-covered $Ni_2P(001)$ (O2_$Ni_2P(001)$) in comparison with experiments.[a]

	Cu(111)	Ni(111)	Ni_2P	O2_Ni_2P
E_{CO}	−0.67, *−0.53* [49]	−1.74, *−1.55* [50]	−1.58 (1)	−1.02 (1)
E_{H_2}	−0.23, ***−0.10*** [51]	−1.28, ***−1.02*** [51]	−1.08 (1)	−0.65 (top of O)
E_{H_2O}	−0.16, ***−0.18*** [9]	−0.47	−0.22 (3)	−0.35 (3)
E_{OH}	−2.68, ***−2.85*** [9]	−3.31	−3.07 (1)	−2.72 (1)
E_{O_2}	−3.50, *−3.82* [52]	−4.78, ***−4.57*** [43]	−4.79 (6)	−2.49 (1)
E_{CO_2}	0.11, ***−0.09*** [9]	−0.05	0.09	>0

[a] Normal italic values are from other experiments [49,50,52] and bold italic values come from other theoretical calculations [9,43,51]. The number in parentheses represents the preferential adsorption site for each adsorbate and the corresponding configuration for each number is shown in Fig. 1. $E_{X_2} = 2E(X^*) - 2E(\text{surf}) - E(X_2)$ for H_2 and O_2 adsorption, $E_Y = E(Y^*) - E(\text{surf}) - E(Y)$ for the other adsorbates. O2_$Ni_2P(001)$ refers to a the $Ni_2P(001)$ surface covered by 2/3 of a ML of atomic O at the Ni–P bridge sites. The adsorbate coverage on Cu(111) and Ni(111) is 1/4 of a ML and 1/3 of a ML on $Ni_2P(001)$ and O2_$Ni_2P(001)$.

Table 2
Calculated energies (eV) for the adsorptions on the different sites of the $Ni_2P(001)$ surface at coverage of 1/3ML.[a]

	Ni site			P sites	Ni–P hybrid sites	
	1	2	3	4	5	6
E_{CO}	−1.58	−1.50	−1.35	−0.23	→2	→1
E_{H_2}	−1.08	→1	→1	−0.52	→1	−0.53
E_{H_2O}	→3	–	−0.22	>0	–	–
E_{OH}	−3.07	−2.89	→1	−2.76	→2	→4
E_{O_2}	−3.87	–	–	→6	→6	−4.79
E_{CO_2}	→3	–	0.09	–	–	>0

[a] The number the preferential adsorption site for each adsorbate, which is shown in Fig. 1. The arrow represents a spontaneous transformation to adsorption on the sites after the arrow.

the hollow site of the Ni(111) surfaces. H_2O and CO_2 bond weakly at the top sites. This is consistent with experiments [54–56] which indicate the binding of H_2O and CO_2 on metal surfaces as a physisorption. For all of the adsorbates, one can see in Table 1 that the interactions with Ni(111) are stronger than with Cu(111).

Table 2 shows the calculated adsorption energies at different sites of the $Ni_2P(001)$ surface including the Ni sites, the P sites, and the Ni–P hybrid sites (Fig. 1). Most of the adsorbates (H_2, CO, OH, H_2O and CO_2) favor the same adsorption site as on Ni(111). The most stable site for H adsorption is Ni hollow site ("1" in Fig. 1) with an adsorption energy of −1.08 eV, which is slightly weaker than that of Ni(111) (−1.28 eV). Similarly, weaker interactions at the Ni hollow sites of $Ni_2P(001)$ are also observed for the other adsorbates. According to our previous studies [28], this is due to an electronic effect, since the Ni atoms of $Ni_2P(001)$ have a d-band center (−1.77 eV, Fig. 6) lower than that of the atoms in Ni(111) (−1.40 eV, Fig. 6) [57,58]. As a result of an ensemble effect, the number of active Ni sites decreases (Fig. 1). Although the P sites and the Ni–P sites ("6" in Fig. 1) also interact with H, the corresponding binding energy is 0.5 eV weaker than that at the Ni hollow sites (Tables 1 and 2). CO and OH also prefer the Ni hollow site (adsorption energies of −1.58 and −3.07 eV, respectively), and in contrast the adsorption at the P sites is weaker (the adsorption energy of −0.23 and −2.76 eV, respectively). Both H_2O and CO_2 only stay at the top of a Ni site with a very weak binding energy as in the cases of Ni(111) and Cu(111). Atomic O is an exception. The most stable site for the adsorption of O is the Ni–P bridge site ("6" in Fig. 1), which is 0.92 eV stronger than the adsorption at the Ni hollow site. On the Ni–P site, oxygen interacts mainly with the P centers. This is due to a strong overlap between the s, p orbitals of O and P (Fig. 6) that is accompanied by a large transfer of electron density from P to O. In addition, the P atom bonded with O shifts outwards the surface by more than 0.2 Å, which also gives rise to a strong O–P interaction. Overall, one can see in Table 2

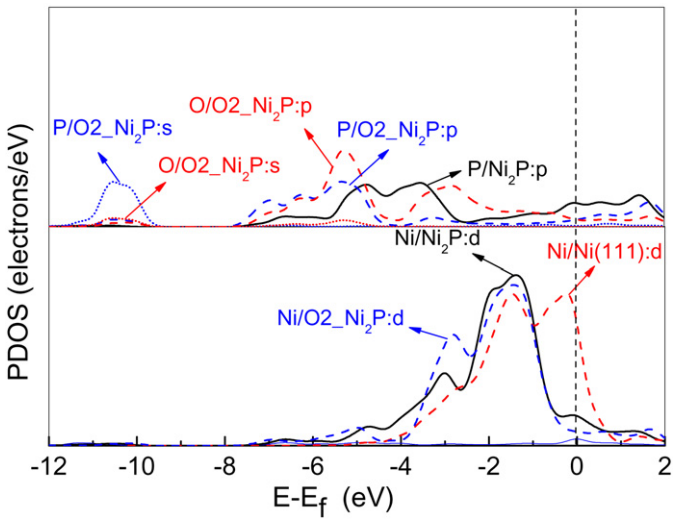

Fig. 6. (Color) Partial density of states (PDOS) of the Ni(111), $Ni_2P(001)$, O2_$Ni_2P(001)$ surfaces.

that the pure Ni sites of $Ni_2P(001)$ bond strongly with the adsorbates, while the less active P sites or the Ni–P hybrid sites also show some adsorption activities. We will see in the following that, the P or Ni–P hybrid sites play an important role during the reaction. This is different from the pure Ni(111) surface, where plenty of active metal hollow sites are available.

3.2.2. WGS reaction on the $Ni_2P(001)$ surface

There have been two pathways proposed regarding the mechanism for the WGS: a regenerative redox mechanism and an associative mechanism [10]. In the redox mechanism, successive oxidation and reduction of the surface occurs as follows:

$$CO + {}^* \leftrightarrow {}^*CO, \quad (1)$$

$$H_2O + {}^* \leftrightarrow H_2O^*, \quad (2)$$

$$H_2O^* + {}^* \leftrightarrow HO^* + H^*, \quad (3)$$

$$HO^* + {}^* \leftrightarrow H^* + O^*, \quad (4)$$

$$CO^* + {}^*O \leftrightarrow {}^*CO_2 + {}^*, \quad (5)$$

$${}^*CO_2 \leftrightarrow CO_2 + {}^*, \quad (6)$$

$$2H^* \leftrightarrow H_2 + 2^*. \quad (7)$$

Here "∗" represents a surface site, and therefore "X∗" stands for the adsorbate bonded to this site. Water dissociates into adsorbed oxygen and hydrogen atoms, and the adsorbed oxygen is then titrated by CO. The associative mechanism involves reaction through an adsorbed intermediate species such as formate (HCOO), carbonate (CO_3), or carboxyl (HOCO). For instance, the dissociated OH reacts with CO to form formate

$$HO^* + CO^* \leftrightarrow HCOO^{**} \quad (8a)$$

or carboxyl

$$HO^* + CO^* \leftrightarrow HOCO^* + {}^*, \quad (8b)$$

which eventually dissociate completely

$$HCOO^{**} \leftrightarrow H^* + CO_2 + {}^*, \quad (9a)$$

$$HOCO^* \leftrightarrow H^* + CO_2, \quad (9b)$$

to form CO_2, H_2 and water. Here, the carbonate intermediate is not included in this study, as it is usually observed when metal oxides are involved [11]. The XPS data discussed in the previous section does not provide a clear evidence for the participation of HCOO or CO_3 in the main reaction pathway for the WGS on $Ni_2P(001)$.

Fig. 7 displays the calculated potential energy diagram for the WGS reaction on $Ni_2P(001)$. The energies are expressed relative to the clean surface, a free CO molecule and H_2O molecule in the gas phase. The adsorptions of CO (1) and H_2O (2) are both exothermic with an energy release of 1.80 eV (Fig. 7A). Water dissociation (3) on $Ni_2P(001)$ is also an exothermic step with the reaction energy (ΔE_3) of −0.48 eV and the corresponding barrier (ΔEa_3) is +1.29 eV. As indicated before, there are several possibilities for the next step, where the reaction intermediates can be O* (4), HCOO** (8a) or HOCO* (8b). We carry out extensive transition state (TS) calculations to find the energy barrier for each of these three reactions. The calculated barriers are shown in Table 3 and the configurations of the corresponding transition states are included in Fig. 7B. In the present study, two factors are considered to determine the optimal reaction mechanism. One is the high stability of the reaction intermediate; the other is the low reaction barrier. The results in Fig. 7A show that *CO + *H + *O is more stable than HOCO* and HCOO* by at least 0.58 eV. In addition, the reaction barrier to produce O by OH splitting (4) is lower than that for the formations of HOCO* ($\Delta Ea_{8b} = +2.55$ eV) and HCOO* ($\Delta Ea_{8a} = +4.49$ eV) (Table 3). Given that, the WGS on a clean $Ni_2P(001)$ should follow the redox mechanism, which gives the lowest barrier of $\Delta Ea_4 = +1.76$ eV. In contrast, the associative mechanism is not likely, as the involved formate and carboxyl intermediates are less stable and more difficult to produce. Here, our calculations also showed that the HCOO* formation is actually controlled by the O–H bond cleavage. As seen in Fig. 7B (d), the corresponding transition state is always associated with the elongated O–H bond. Interacting with *CO species, the produced *O yields *CO_2 (5). This is the first endothermic and the most difficult step with the energy loss of +0.44 eV and the highest barrier of +2.23 eV. Finally, the desorptions of CO_2 and H_2 (6), (7) are also up-hill reactions with the energy cost of +1.10 eV. It is known that temperature and pressure will particularly affect the chemical potential of gas-phase molecules. Desorption processes, such as a $2H^* \rightarrow H_2$ reaction, are driven by a large entropy term at elevated temperatures, so the endothermic nature of the final step on $Ni_2P(001)$, or O-covered $Ni_2P(001)$ as we will see below, does not represent a significant problem. Overall, the WGS on $Ni_2P(001)$ is dominated by a redox mechanism and CO oxidation into CO_2 is the rate-limiting step (rls).

It has already been shown in previous studies [8] that Cu is a better WGS catalyst than Ni. The strong CO interaction with the Ni surface leads to a CO-poisoning under the working conditions, especially with a high CO/H_2O ratio, which blocks the Ni sites from water dissociation and the rest of the WGS reaction. The high coverage of CO on Ni(100) also leads to deactivation by the deposition of carbon through the Boudouard reaction, 2CO(ads) → C(ads) + CO_2 (gas) [7]. Therefore, a low WGS activity and small amount of oxygen were observed experimentally (Fig. 4). However, this is not the case for $Ni_2P(001)$, where a substantial amount of oxygen was detected after the WGS reaction (Fig. 4). The calculated results in Table 1 show that due to a weak ligand effect [28], the bonding strength of $Ni_2P(001)$ to an adsorbate like CO is slightly weaker than that of Ni(111) and much stronger than that of Cu(111). As a result, the CO-poisoning of $Ni_2P(001)$ is also expected but an ensemble effect due to the presence of P prevents the deposition of carbon on the surface through the Boudouard reaction. According to our calculations (Table 2), CO prefers the Ni sites rather than the P sites or Ni–P hybrid sites, which, as we will see below, are involved in water dissociation by providing strong bonding to the dissociated OH, O and H. Do this weak ligand effect and the direct participation of the P sites in water dissociation make Ni_2P a better WGS catalyst than Cu? According to our previous work [29],

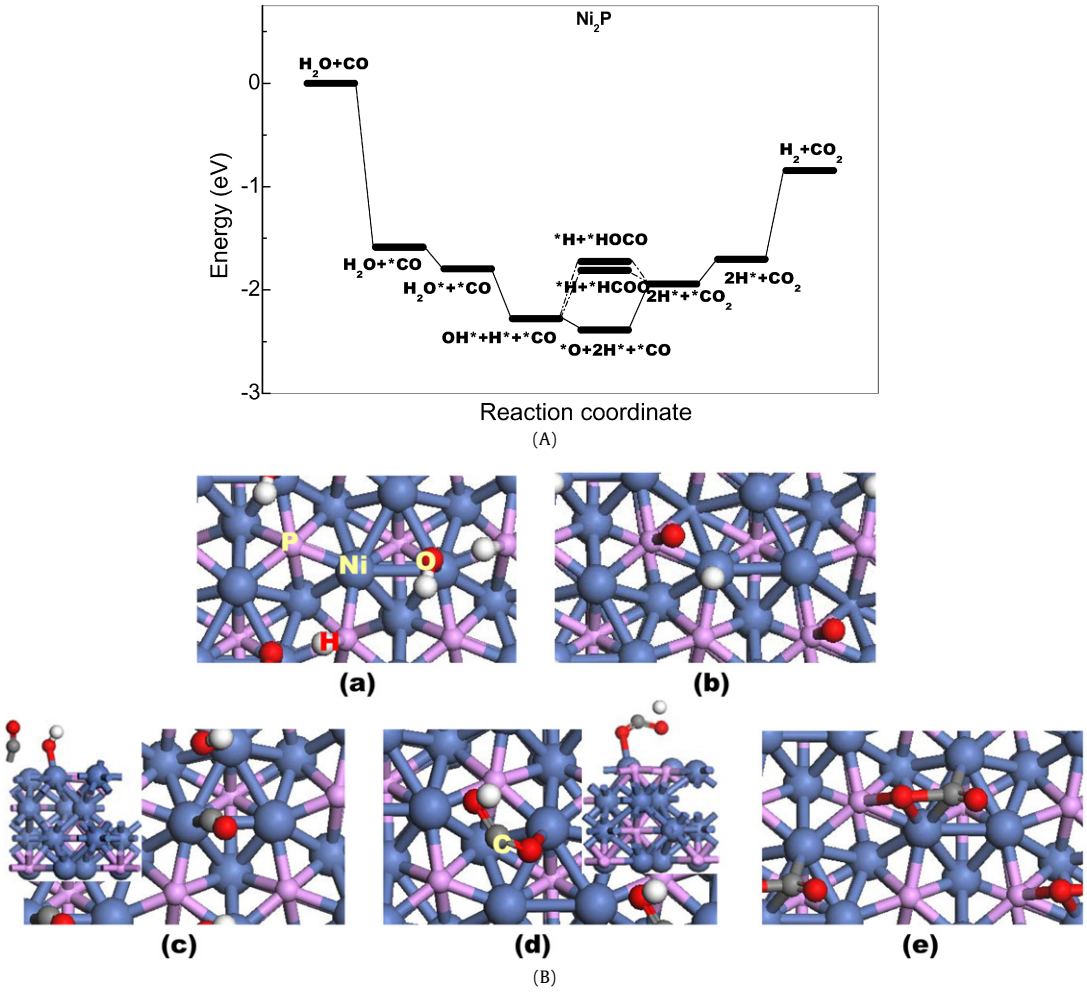

Fig. 7. (A) Calculated potential energy diagram for the WGS reaction on the $Ni_2P(001)$ surface. The energies in the figure are expressed with respect to bare $Ni_2P(001)$ and free CO and H_2O molecules in gas phase. (B; color) Top views of the geometries of the transition states involved in the WGS reaction on $Ni_2P(001)$: (a) transition state for water dissociation ($H_2O^* + {}^*HO^* + H^*$); (b) transition state for OH dissociation (${}^*OH + {}^* \rightarrow O^* + H^*$); (c) transition state for carboxyl formation ($CO^* + {}^*OH \leftrightarrow HOCO^* + {}^*$) (inset: side view); (d) transition state for formate formation ($CO^* + {}^*OH \leftrightarrow HCOO^{**}$) (inset: side view); (e) transition state for CO_2 formation ($CO^* + O^* \leftrightarrow CO_2^*$).

water dissociation (3) is the rls for the WGS reaction on Cu(111) with a barrier of 1.54 eV. In the case of $Ni_2P(001)$, the barrier is lowered by 0.25 eV and the corresponding transition site is bridging the Ni and P sites (a, Fig. 7B). However, one can see in Table 1 that for atomic oxygen, the adsorption at the Ni–P bridge site on $Ni_2P(001)$ is stronger than on Cu(111) by more than 1 eV. As a result, the O removal from $Ni_2P(001)$ in the form of CO_2 is so slow that it becomes the rls with a barrier of +2.23 eV. Given that, our DFT calculations imply that the WGS reaction on $Ni_2P(001)$ does not proceed as well as on Cu. This conflicts with our experiments which show a better WGS activity on Ni_2P than on Cu (Fig. 4). To understand this, we have considered the role of adsorbed oxygen. Due to the fact that the O–Ni_2P interaction is too strong to be broken by CO oxidation, $Ni_2P(001)$ is easily covered with O during the WGS reaction (Fig. 2).

3.2.3. Effect of adsorbed oxygen on the WGS activity of $Ni_2P(001)$

The XPS and ISS data discussed in Section 3.1 point to a significant amount of oxygen covering the $Ni_2P(001)$ substrate under reaction conditions. The oxygen is mainly bonded to the P sites and its exact adsorption geometry is not known. The bottom of Fig. 8 shows adsorption geometries obtained with DFT after depositing different coverages of O on $Ni_2P(001)$. As in the case of the experimental measurements, the DFT calculations point to a strong

Table 3
Calculated reaction barriers (eV) for the important elementary steps involved in WGS reaction on the $Ni_2P(001)$ and O2_$Ni_2P(001)$ surfaces.[a]

	Ni_2P	O2_Ni_2P
$H_2O^* + {}^* \leftrightarrow HO^* + H^*$	1.29	0.92
${}^*OH + {}^* \leftrightarrow O^* + H^*$	1.76	3.71
$CO^* + {}^*OH \leftrightarrow HOCO^* + {}^*$	2.55	1.15
$CO^* + {}^*OH \leftrightarrow HCOO^{**}$	4.49	4.22
$CO^* + O^* \leftrightarrow CO_2^* + {}^*$	2.23	–
$HOCO^* + {}^* \leftrightarrow CO_2^* + H^*$	–	0.31

[a] O2_$Ni_2P(001)$ represents the $Ni_2P(001)$ surface covered by 2/3ML of O at the Ni–P bridge sites.

interaction between the O and P sites. We calculated the differential adsorption energy of O on $Ni_2P(001)$:

$$\Delta E_0 = E(n\mathrm{O/Surf}) - E\big[(n-1)\mathrm{O/Surf}\big] - 1/2E(\mathrm{O_2}), \quad (10)$$

where "n" is the number of O atoms adsorbed per supercell ($1 \leqslant n \leqslant 3$). In Fig. 8, we plot the results for three different oxygen coverages and values of "n." The more negative the value of E_0, the stronger the O bonding to the surface. The top panel in Fig. 8 displays the calculated E_0 at different coverages, and the corresponding geometries are also included. As indicated before, at low coverage (1/3ML), O binds very strongly on the Ni–P bridge site ($\Delta E_0 = -2.39$ eV) interacting mainly with the P center. At 2/3ML, the other Ni–P bridge site is preferred, and the O binding en-

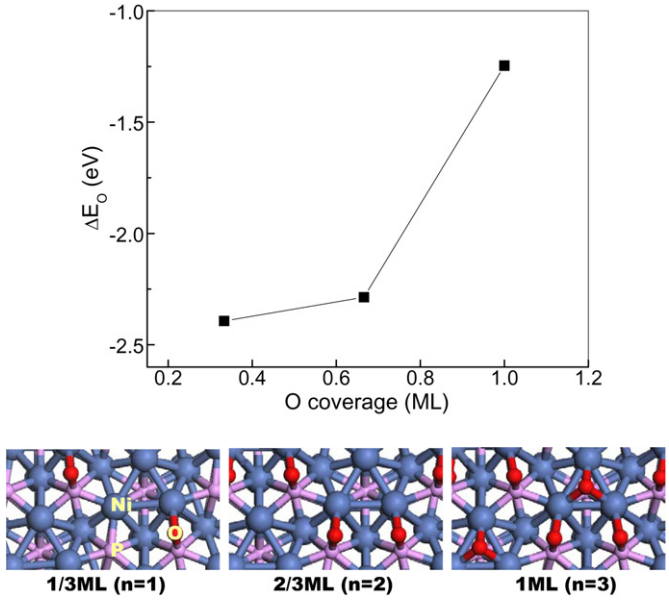

Fig. 8. (Color) Calculated O adsorption energy on $Ni_2P(001)$ at different coverage; the corresponding geometries are shown at the bottom of the figure. ΔE_0 is expressed as Eq. (10). We have considered three different oxygen coverages and values of "n" in Eq. (10).

ergy changes slightly ($\Delta E_0 = -2.28$ eV). Only upon going from 2/3ML to 1ML, a significant decrease of O binding energy is observed ($\Delta E_0 = -1.25$ eV). That is, O is able to strongly adsorb on $Ni_2P(001)$ up to 2/3ML due to the high activity of the P surface atoms towards O. After all the Ni–P sites are occupied, further addition of O results in the occupation of the less active Ni hollow site, and the O–Ni_2P interaction is weakened greatly. That is, the full oxidation of $Ni_2P(001)$ is highly activated, and the Ni hollow sites should survive under WGS reaction conditions. Our calculations agree well with the experiments (see Section 3.1), where the presence of adsorbed O and O–P interactions were observed in XPS spectra taken after performing the WGS reaction on $Ni_2P(001)$. Based on this, we take a further step to investigate the WGS on the $Ni_2P(001)$ surface covered by 2/3ML of O at the Ni–P bridge sites (O2_$Ni_2P(001)$ in our notation). Although the experimental measurements cannot determine the exact coverage of O, O2_$Ni_2P(001)$ is selected due to its high stability according to the DFT calculations (Fig. 8).

As shown in Table 1, most of the adsorbates (CO, CO_2, O_2, H_2 and OH) bind more weakly with the O-covered surface. Compared to $Ni_2P(001)$, the presence of O deactivates the Ni sites of O2_$Ni_2P(001)$, which is probably a consequence of electron transfer from Ni to O and therefore a downward-shift of the d-band of Ni (Fig. 6). In addition, the O atoms in the surface also introduce repulsions to these O-containing adsorbates. The only species that bonds O2_$Ni_2P(001)$ as strongly as $Ni_2P(001)$ is H_2O (Table 1). Although the atop of Ni is also preferred in the case of O2_$Ni_2P(001)$, H_2O tilts towards the O atom in the surface and form a weak H bond, which helps to stabilize the molecule.

Fig. 9A shows the potential energy diagram for the WGS reaction on O2_ $Ni_2P(001)$. Differently from $Ni_2P(001)$, the reaction on O2_$Ni_2P(001)$ follows the similar trend as that of Cu [8,9,29] and the variation in energy throughout the pathway is much smaller. The water dissociation (3) is an endothermic reaction ($\Delta E_3 = +0.55$ eV), rather than exothermic, however, the corresponding activation barrier is lower ($\Delta Ea_3 = +0.92$ eV, Table 3) compared to the case of $Ni_2P(001)$. It is attributed to the strong O ↔ H interaction (Fig. 9B). Our calculations show that the adsorption of H on top of O in the surface of O_$Ni_2P(001)$ is 0.12 eV stronger than that on the Ni hollow site (Table 1). Different from the case of $Ni_2P(001)$, on O2_$Ni_2P(001)$, HCOO* is more stable than HOCO*, but the energy difference between *CO + *H + *O and HOCO* is rather small (0.3 eV). *CO + *H + *O is the least stable set of species due to a big weakening of O adsorption on O2_$Ni_2P(001)$ (see Table 1). In addition, as shown in Table 3, the formation of HOCO* on O2_$Ni_2P(001)$ ($\Delta Ea_{8b} = +1.15$ eV) is much more favorable than the formations of HCOO* ($\Delta Ea_{8a} = +4.22$ eV) and O* ($\Delta Ea_4 = +3.71$ eV). Given the lowest stability and the high formation barrier, the *CO + *H + *O species is clearly ruled out as an intermediate in the WGS reaction. HCOO* is slightly more stable than HOCO*, however, we also notice that the production of HCOO* has to cost 3.07 eV more energy than that of HOCO*. This makes HOCO* the most favorable intermediate. Similar to the case of $Ni_2P(001)$, the transition from *CO+ *OH to HCOO* is controlled by the O–H bond cleavage (see Figs. 9d and S1). That is, the WGS reaction on O2_$Ni_2P(001)$ probably adopts an associative mechanism via carboxyl, which dissociates into CO_2 and *H (9b) with an energy gain of −1.27 eV and a barrier of +0.31 eV. Therefore, the formation of carboxyl (8b) should be the rls, which corresponds to a barrier 0.39 eV lower than that of water dissociation on Cu. Therefore, a higher WGS activity is expected for O/Ni_2P than for Cu, and indeed this is seen in experimental measurements (Fig. 4). In our previous work [8,29], we developed a micro-kinetic model based on the DFT calculations, which allowed us to estimate the overall WGS rate. The results show that the overall rate is well correlated with the barrier of the rls: the lower the barrier is, the faster the WGS reaction runs. Therefore, the difference in the barrier for the rls gives a semi-quantitative description of the trend in the overall activity from one system to the next, which is our interest here. Given that, the WGS reaction on O2_$Ni_2P(001)$ (barrier of rls: 1.15 eV) proceeds better than that on $Ni_2P(001)$ (barrier of rls: 2.23 eV).

In Fig. 4, the pure transition metals, Ni and Cu, are not highly active catalysts for the WGS reaction. Ni bonds the intermediates too strongly to be removed from the surface. Cu is the best metal catalyst for the WGS reaction because displays a moderate bonding towards the reactants, intermediates and products [14]. In spite of the deactivation introduced by P, Ni_2P binds the WGS adsorbates much stronger than Cu, and the clean $Ni_2P(001)$ does not catalyze the WGS reaction as well as Cu. Species such as O and S interact strongly with nickel phosphide without decreasing or removing its catalytic activity [28,34,36]. In fact, our results from both experiment and theory show that the good behavior of Ni_2P is associated with the Ni oxy-phosphide formed as a result of strong O ↔ P interactions under the WGS reaction conditions. Compared to $Ni_2P(001)$, the presence of oxygen helps in facilitating the water dissociation on O/$Ni_2P(001)$, which is the rls in the case of Cu [9,29]. In Fig. 9B, the dissociation of H_2O is the result of a cooperation of a Ni and O center of the O/$Ni_2P(001)$ surface. In addition, the O atoms in the surface of O/$Ni_2P(001)$ also destabilize the oxygen-containing species (such as CO, O, and OH. See Table 1) by deactivating the Ni sites and providing lateral repulsion, which leads to a facile removal of CO (Table 3). This is similar to the case of the [NiFe] hydrogenase enzyme, where the active sites also involve the combination of a metal and a light atom [30]. Such a combination of elements can do chemistry with the reactants and does not bind intermediates and products too strongly, obeying Sabatier principle. Given that, we speculate that the promotion effect of Cs on the WGS activity of $Ni_2P(001)$ is associated with increasing the amount of adsorbed O, as observed experimentally (Fig. 4), to help in dissociating water and removing CO. In the case of Cu(100) or Cu(111), there are only metal centers with a moderate reactivity and these systems are less active WGS catalysts than O/$Ni_2P(001)$. However, the WGS activity of the copper surfaces is enhanced by adding Cs as a promoter [5], with the alkali metal be-

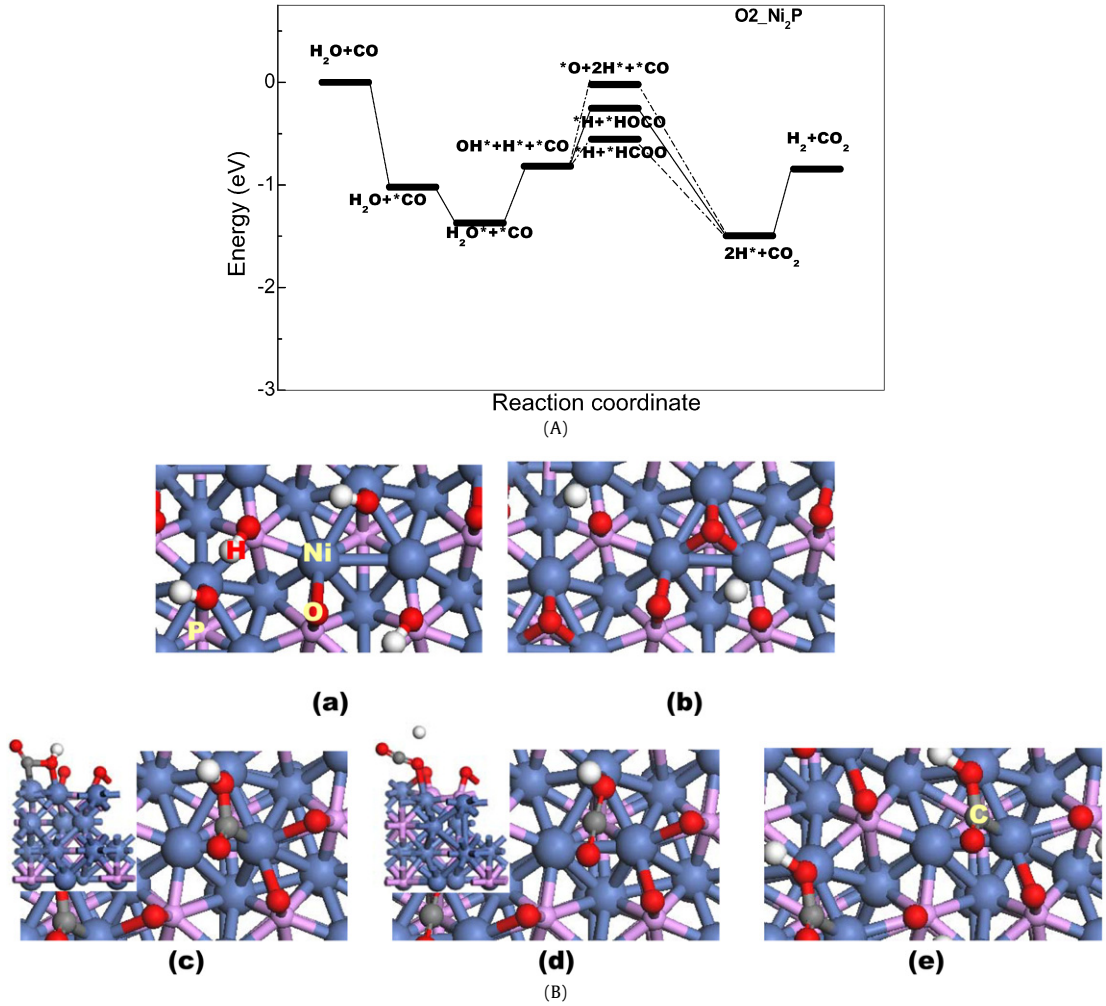

Fig. 9. (A) Calculated potential energy diagram for the WGS reaction on the O-covered $Ni_2P(001)$ surface. The energies in the figure are expressed with respect to $Ni_2P(001)$ covered by 2/3ML of O and free CO and H_2O molecules in gas phase. (B, color) Top views of the geometries of the transition states involved in the WGS reaction on O-covered $Ni_2P(001)$: (a) transition state for water dissociation ($H_2O^* + {}^* \leftrightarrow HO^* + H^*$); (b) transition state for OH dissociation ($^*OH + {}^* \leftrightarrow O^* + H^*$); (c) transition state for carboxyl formation ($CO^* + {}^*OH \leftrightarrow HOCO^* + {}^*$; inset: side view); (d) transition state for formate formation ($CO^* + {}^*$ $OH \leftrightarrow HCOO^{**}$; inset: side view); (e) transition state for CO_2 formation ($HOCO^* \leftrightarrow CO_2 + H^*$).

coming $CsO_x/Cs(OH)_y$ under reaction conditions and providing the O sites necessary for an efficient dissociation of water. Similar to the case of Ni_2P, the formation of a Mo oxy-carbide on the surface of Mo_2C is responsible for a high WGS activity [29]: the oxygen atoms on the surface help to dissociate water. Our results imply that the high performances of catalysts in the WGS rely heavily on the direct participation of oxygen by providing moderate bonding to intermediates and an indirect participation by tuning the activity of metal sites.

4. Summary and conclusion

Both experimental and theoretical studies were employed to investigate the WGS activity of the $Ni_2P(001)$ surface. Our kinetic measurements showed that the $Ni_2P(001)$ substrate displays a WGS activity significantly larger than that of Ni(100) or even Cu(100). Under reaction conditions, most of the P sites of $Ni_2P(001)$ are covered with oxygen. The addition of Cs to the nickel phosphide surface increases the saturation coverage of oxygen and enhances catalytic activity. As in the case of a [NiFe] hydrogenase enzyme, the active sites of $O/Ni_2P(001)$ involve the combination of a metal and a light atom. This configuration of the active sites leads to significant changes in the reaction mechanism with respect to that on Ni(100) or Cu(100). The O atoms on the $Ni_2P(001)$ surface facilitate the WGS reaction in both direct and indirect ways. On one hand, O helps to lower the barrier for water dissociation; on the other hand, it also deactivates the Ni sites in the surface to provide moderate bonding to the adsorbates. Our results imply that the high performances of catalysts in the WGS rely heavily on the cooperation between oxygen and metal centers with moderate activity.

Acknowledgments

The research carried out at Brookhaven National Laboratory was supported by the US Department of Energy, Division of Chemical Sciences, under Contract DE-AC02-98CH10886. K.N. thanks the Nippon Foundation for Materials Science for research grants that made possible part of this work. The authors are grateful to J. Evans for his help in the design of the reaction cell in which kinetic studies were carried out and to T. Asakura for the initial cleaning and preparation of the $Ni_2P(001)$ crystal.

Supplementary material

The online version of this article contains additional supplementary material.

Please visit DOI: 10.1016/j.jcat.2009.01.006.

References

[1] D.S. Newsome, Catal. Rev. Sci. Eng. 21 (1980) 275.
[2] M.V. Twigg (Ed.), Catalyst Handbook, second ed., Wolfe, England, 1989.
[3] Q.S. Liu, Q.C. Zhang, W.P. Ma, R.X. He, L.J. Kou, Z.J. Mou, Prog. Chem. 17 (2005) 389.
[4] H. Bohlbro, M.H. Jørgensen, Chem. Eng. World 5 (1970) 46.
[5] C.T. Campbell, B.E. Koel, Surf. Sci. 186 (1987) 393.
[6] J. Nakamura, J.M. Campbell, C.T. Campbell, Faraday Trans. 86 (1990) 2725.
[7] J.A. Rodriguez, D.W. Goodman, Surf. Sci. Rep. 14 (1991) 1.
[8] P. Liu, J.A. Rodriguez, J. Chem. Phys. 126 (2007) 164705.
[9] A.A. Gokhale, J.A. Dumesic, M. Mavrikakis, J. Am. Chem. Soc. 130 (2008) 1402.
[10] C. Rhodes, G.J. Hutchings, A.M. Ward, Catal. Today 23 (1995) 43.
[11] R. Burch, Phys. Chem. Chem. Phys. 8 (2006) 5483.
[12] D.L. Trimm, Appl. Catal. A 296 (2005) 1.
[13] L.C. Grabow, A.A. Gokhale, S.T. Evans, J.A. Dumesic, M. Mavrikakis, J. Phys. Chem. C 112 (2008) 4608.
[14] N. Schumacher, A. Boisen, S. Dahl, A.A. Gokhale, S. Kandoi, L.C. Grabow, J.A. Dumesic, M. Mavrikakis, I. Chorkendorff, J. Catal. 229 (2005) 265.
[15] J.A. Rodriguez, P. Liu, X. Wang, W. Wen, J. Hanson, J. Hrbek, M. Pérez, J. Evans, J. Catal. Today (2009), doi: 10.1016/j.cattod.2008.08.022, in press.
[16] Q. Fu, H. Saltsburg, M. Flytzani-Stephanopoulos, Science 301 (2003) 935.
[17] E.S. Bickford, S. Velu, C.S. Song, Catal. Today 99 (2005) 347.
[18] S.Y. Choung, M. Ferrandon, T. Krause, Catal. Today 99 (2005) 257.
[19] X.S. Liu, W. Ruettinger, A.M. Xu, R. Farrauto, Appl. Catal. B 56 (2005) 69.
[20] C.H. Kim, L.T. Thompson, J. Catal. 230 (2005) 66.
[21] X. Wang, R.J. Gorte, J.P. Wanger, J. Catal. 212 (2002) 225.
[22] Y. Sato, K. Terada, S. Hasegawa, T. Miyao, S. Naito, Appl. Catal. A 296 (2005) 80.
[23] W. Wen, J. Liu, M.G. White, N. Marinkovic, J.C. Hanson, J.A. Rodriguez, Catal. Lett. 113 (2007) 1.
[24] J.A. Rodriguez, P. Liu, J. Hrbek, J. Evans, M. Pérez, Angew. Chem. Int. Ed. 46 (2007) 1329.
[25] J.A. Rodriguez, S. Ma, P. Liu, J. Hrbek, J. Evans, M. Pérez, Science 318 (2007) 1757.
[26] D.J. Moon, J.W. Ryu, Catal. Lett. 92 (2004) 17.
[27] Q. Li, X. Hu, Phys. Rev. B 74 (2006) 035414.
[28] P. Liu, J.A. Rodriguez, T. Asakura, J. Gomes, K. Nakamura, J. Phys. Chem. B 109 (2005) 4575.
[29] P. Liu, J.A. Rodriguez, J. Phys. Chem. B 110 (2006) 19418.
[30] P. Liu, J.A. Rodriguez, J. Am. Chem. Soc. 127 (2005) 17871.
[31] M. Golam-Moula, S. Suzuki, W.J. Chun, S. Otani, S.T. Oyama, K. Asakura, Chem. Lett. 35 (2006) 90.
[32] M.G. Moula, S. Suzuki, W.J. Chun, S.T. Oyama, K. Asakura, S. Otani, Surf. Interface Anal. 38 (2006) 1611.
[33] K. Kinoshita, G.H. Simon, T. Konig, M. Heyde, H.J. Freund, Y. Nakagawa, S.T. Oyama, S. Ohtani, K. Asakura, Jpn. J. Appl. Phys. 47 (2008) 6088.
[34] S.T. Oyama, J. Catal. 216 (2003) 343.
[35] D. Kanama, S.T. Oyama, S. Otani, D.F. Cox, Surf. Sci. 552 (2004) 8.
[36] Y.K. Lee, Y. Shu, T.S. Oyama, Appl. Catal. A 322 (2007) 191.
[37] K.A. Layman, M.E. Bussell, J. Phys. Chem. B 108 (2004) 15791.
[38] M.C. Payne, D.C. Allan, T.A. Arias, J.D. Johannopoulus, Rev. Mod. Phys. 64 (1992) 1045.
[39] P. Liu, J.A. Rodriguez, J.T. Muckerman, J. Hrbek, Phys. Rev. B 67 (2003) 155416.
[40] P. Liu, J.A. Rodriguez, Catal. Lett. 91 (2003) 247.
[41] D. Vanderbilt, Phys. Rev. B 41 (1990) 7892.
[42] H.J. Monkhorst, J.D. Pack, Phys. Rev. B 12 (1976) 5188.
[43] B. Hammer, L.B. Hansen, J.K. Nørskov, Phys. Rev. B 59 (1999) 7413.
[44] J. Haglund, A.F. Guillermet, G. Grimvall, M. Korling, Phys. Rev. B 48 (1993) 11685.
[45] J.A. Rodriguez, J.Y. Kim, J.C. Hanson, S.J. Sawhill, M.E. Bussell, J. Phys. Chem. B 107 (2003) 6276, and references therein.
[46] C.D. Wagner, W.M. Riggs, L.E. Davis, J.F. Moulder, G. Muilenberg (Eds.), Handbook of X-ray Photoelectron Spectroscopy, Perkin–Elmer, Eden Prairie, MN, 1977.
[47] X. Wang, J.A. Rodriguez, J.C. Hanson, M. Pérez, J. Evans, J. Chem. Phys. 123 (2005) 221101.
[48] J.A. Rodriguez, P. Liu, J. Hrbek, M. Pérez, J. Evans, J. Mol. Catal. A 281 (2008) 59.
[49] I. Bönike, W. Kirstein, S. Spingzig, F. Thieme, Surf. Sci. 313 (1994) 231.
[50] H. Ibach, W. Erley, H. Wanger, Surf. Sci. 92 (1980) 29.
[51] J.K. Nørskov, T. Bligaard, A. Logadottir, J.R. Kitchin, J.G. Chen, S. Pandelov, U. Stimming, J. Electrochem. Soc. 152 (2005) J23.
[52] E. Shustorovich, Adv. Catal. 37 (1990) 101.
[53] J.F. Paul, P. Sautet, Surf. Sci. 356 (1996) L403.
[54] P.A. Thiel, T.E. Madey, Surf. Sci. Rep. 7 (1987) 211.
[55] J.A. Rodriguez, W.D. Clendening, C.T. Campbell, J. Phys. Chem. 93 (1989) 5238.
[56] F.H.P.M. Habraken, E.Ph. Kieffer, G.A. Bootsma, Surf. Sci. 83 (1979) 45.
[57] J. Greeley, J.K. Nørskov, M. Mavrikakis, Annu. Rev. Phys. Chem. 53 (2002) 319.
[58] B. Hammer, J.K. Nørskov, Adv. Catal. 45 (2000) 71.